Published in Journal of Applied Physics 96, issue 1, 7-11, 2004
which should be used for any reference to this work

Practical and theoretical modal analysis of photonic crystal waveguides

Iwan Märki,[a] Martin Salt, and Hans Peter Herzig
Institute of Microtechnology, University of Neuchâtel, rue A.-L. Breguet, 2, CH-2000 Neuchâtel, Switzerland

We present practical and theoretical, stage-by-stage analysis of light propagation around a 90° corner in a two-dimensional photonic crystal waveguide. Using a series of different samples we quantify the coupling efficiency between the conventional ridge waveguide and the photonic crystal waveguide as well as the bending efficiency around the 90° corner. From this, the transmission spectra indicate nearly 90% bending efficiency. We compare the experimental results to the three-dimensional simulated band diagram and field distribution. The propagating defect modes are identified in detail and we show that efficient transmission around sharp bends in photonic crystal waveguides can be achieved for leaky modes above the light line with short photonic crystal sections.

I. INTRODUCTION

Light propagation in photonic crystal waveguides is a topic under intense investigation. By introducing a properly designed line defect in a photonic crystal structure, propagating modes confined within the defect are created.[1–10] Depending on the nature of the guided defect mode, waveguiding with low losses even around sharp bends can be achieved.[11–16] We present thorough experimental and theoretical analysis of light propagation around a 90° corner in a photonic crystal slab. Quantative transmission spectra of samples with different designs are compared to fully three-dimensional (3D) simulations for a more complete understanding of the transmission efficiency, the propagating modes and the coupling between the ridge waveguide and the photonic crystal waveguide. We identify in detail the propagating defect modes and show that efficient transmission around sharp bends can be achieved above the light line. In this article, we concentrate on the modal analysis of the photonic crystal waveguide whereas the experimental results will be presented in more detail elsewhere.

In our case the photonic crystal consists of a square array of cylindrical air holes in a thin silicon membrane surrounded by air. The structure is designed to give rise to a TE-like (in-plane polarization) photonic band gap around $\lambda \sim 1.5\ \mu$m. The design parameters of the photonic crystal structure are the lattice constant $a = 496$ nm, the hole radius $r = 190$ nm and the slab thickness $t = 290$ nm. Our waveguides are fabricated in silicon–on–insulator wafers.[5,17] The thickness of the Silicon slab is defined by oxidation and Hartree–Fock dip. The photonic crystal waveguide structure is then written into a polymethyl methacrylate (PMMA) layer by means of electron beam lithography. Then, we use reactive ion etching (RIE) and deep reactive ion etching (DRIE) to transfer the structure from the PMMA layer into the Silicon. Last buffered hydrofluoric acid vapor etching removes the silicon dioxide layer underneath the Silicon slab forming the membrane [Fig. 1(a)].

[a]Electronic mail: iwan.maerki@unine.ch

Measurements are performed with an optical setup that includes a tunable laser source. TE-polarized light is coupled into a wide (10 μm) ridge waveguide on a SiO_2 substrate using an aspheric lens with a high numerical aperture (NA $=0.65$). Chemically etched end-facets at the input and output of the waveguide greatly reduce scattering of the laser light and allow a better coupling at the input and a very well defined mode profile at the output [Fig. 1(b)]. To measure the transmitted intensity, the light is collected at the output of the waveguide by a microscope objective (NA$=0.35$) and focused onto an InGaAs detector. The tunable laser source allows us to measure the transmission spectrum ranging from 1440 to 1580 nm.

In order to study the effects of ridge waveguide to photonic crystal waveguide modal mismatch and induced modal conversion, we fabricated a series of samples that represent the different subelements of a final photonic crystal bend sample. This allows a better understanding of how each element contributes to the final photonic crystal bend spectrum. The first design is a simple, straight multimode waveguide [Fig. 2(a)] on a SiO_2 substrate with a width of 10 μm and a thickness of 290 nm. It serves as reference for the transmission efficiency.[12] The second design is a straight waveguide with a taper [Fig. 2(b)] that reduces the width to 500 nm, leading to a waveguide section of a length of 25 μm in the middle and again a taper to increase the width back to 10 μm. The 25 μm middle waveguide section is a free-standing membrane and its width is approximately equal to the width of the photonic crystal waveguide defect channel. This second design allows us to observe the influence of the taper-induced modal conversion. The next stage is the insertion of the photonic crystal containing a straight, single line defect (no holes) into the middle of the waveguide [Fig. 2(c)]. The photonic crystal section is again a free-standing membrane due to the under-etching of the SiO_2 substrate through the holes. It has a length of 20 μm and allows us to study the effect of the modal mismatch between the ridge waveguide and the photonic crystal waveguide,[18] as well as losses created by the crystal. Finally, the 90° bend is introduced into the photonic crystal waveguide section [Fig. 2(d)].

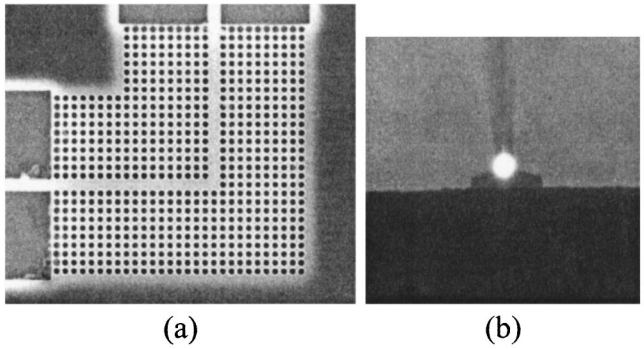

FIG. 1. (a) Scanning electron microscopy image of the 90° bend photonic crystal waveguide. (b) Infrared image of light output after a 90° bend.

II. TRANSMISSION EFFICIENCY AND MODAL ANALYSIS

To obtain the approximate transmission efficiency of the different waveguides, shown in Fig. 3(a), we first remove numerically the periodic Fabry–Pérot interference pattern, which is due to the smooth end-facets. Second, we divide the transmission spectra by the spectrum of the simple, straight, reference waveguide (a) for normalization. This eliminates extrinsic effects of the end injection and most of the spectral response of the measurement optics. Repeated measurement of the same sample and of different samples of the same type has shown that an error of about 10% has to be attributed to the transmission measurements. These errors are due to changes in the alignment of the optical measurement system and due to fabrication-induced variations between the different waveguides.

For the straight waveguide containing the taper and the small width section we observe comparatively high transmission efficiency over the entire measured frequency range in respect to the reference waveguide (a). Therefore we conclude that there are only slight losses induced by the taper in our setup, which indicates a good modal conversion. It also indicates that the majority of the injected light must couple to the lower-order modes of the waveguide. For the straight photonic crystal waveguide channel a high transmission efficiency is observed for the lower frequency range whereas for the higher frequency range the transmission is near to zero. The cutoff frequency is around 1.96×10^{14} Hz. The high transmission efficiency for the lower frequency range indicates a high coupling efficiency with low propagation loss and therefore a small modal mismatch between the ridge waveguide and the photonic crystal waveguide. From the measurement data we have estimated the propagation loss in the photonic crystal section to be 25 dB/mm in the best case. Details of the loss calculation will be presented elesewhere. A transmission efficiency of nearly 90%, which includes ridge waveguide to photonic crystal losses, is observed for the 90° bend waveguide at a frequency of 1.957×10^{14} Hz. It has a bandwidth of $\Delta f\approx2700$ GHz for a transmission efficiency of more than 60%. In Fig. 3(b) we show the fully 3D simulated transmission efficiency for the 90° bend waveguide. The simulation has been performed by a 3D finite integration time domain (FITD) algorithm.[19] The general shape of the simulated transmission spectrum compares relatively well with the measured transmission efficiency. The

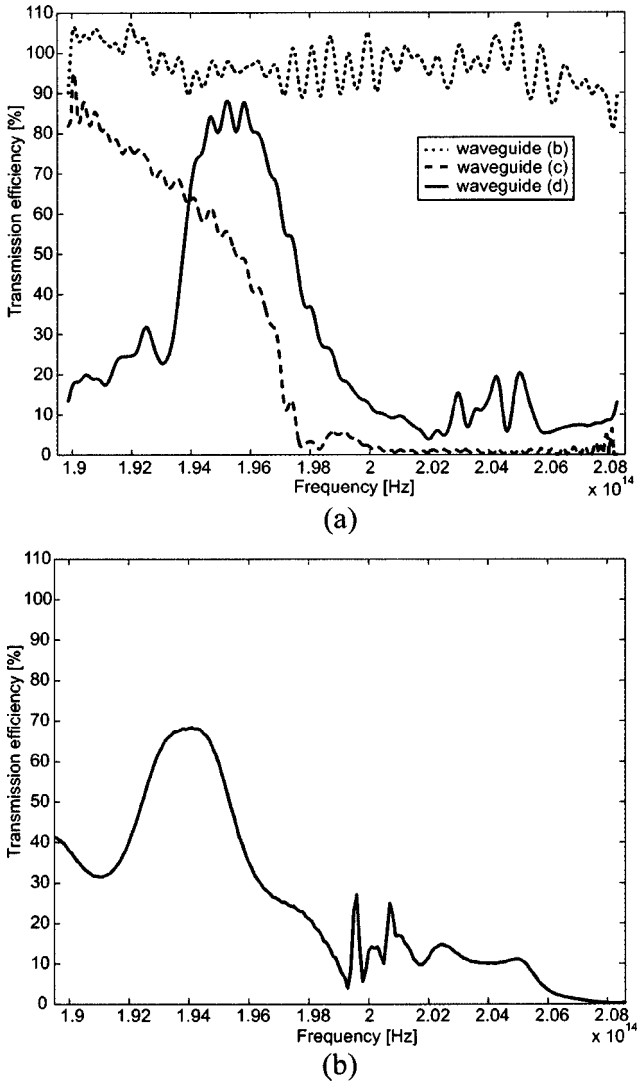

FIG. 3. (a) Transmission efficiency calculated from the measured transmission spectra in reference to the simple, straight ridge waveguide with a width of 10 μm. The rapid fluctuations are due to interference in the optical system that has not been eliminated in the filtering and normalizing process. (b) Fully 3D simulated transmission efficiency for the 90° bend waveguide.

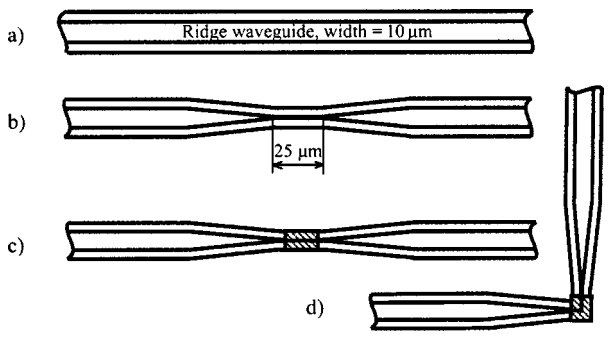

FIG. 2. Designs of the fabricated waveguides: (a) simple straight waveguide (width=10 μm); (b) straight waveguide with taper and narrow width section (width=500 nm); (c) straight waveguide with photonic crystal waveguide (photonic crystal waveguide length=25 μm); and (d) waveguide with 90° bend.

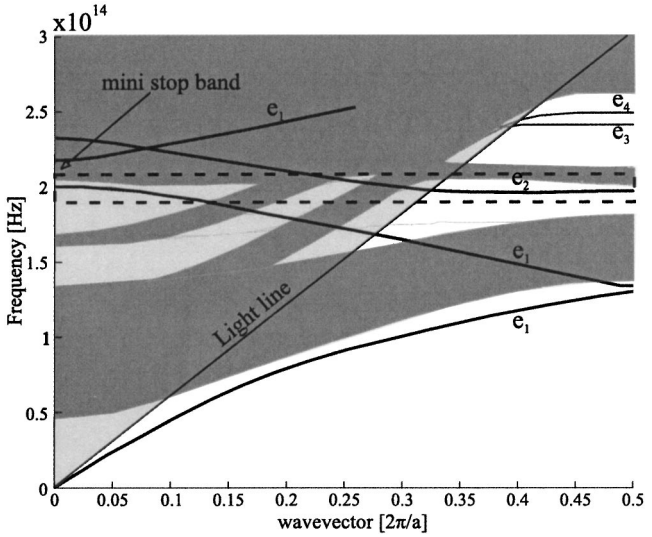

FIG. 4. Computed dispersion diagram for TE-like guided modes in the photonic crystal waveguide. The defect modes are represented by solid black lines and are labeled e_1 and e_2. The dark gray regions correspond to modes of the photonic crystal, which are states that can propagate through the crystal.

observed differences are due to variations between the ideal simulated structure and the fabricated structure. The simulated photonic crystal structure was slightly shorter than the real structure due to the limited calculation capacity. Also, the many parameters (hole radius, lattice period, slab thickness, surface roughness) and the lengthy calculations do not allow rigorous convergence to the response of the real fabricated structure.

For a better understanding of the observed results we introduce the computed dispersion diagram for TE-like modes of the photonic crystal waveguide obtained by a fully three-dimensional calculation.[20] The guided defect modes, shown in Fig. 4, are represented by solid black lines. The dark gray regions correspond to modes of the photonic crystal, which are states that can propagate through the crystal. Guided modes that exist in that region can couple to the states of the photonic crystal and leak energy into it. The light line is indicated by the thin solid black line. Modes above the light line (light gray region) can escape in the vertical direction and therefore can leak energy into the air.

The first guided mode, labeled e_1, is a laterally even mode.[9] Its dispersion is comparable to the folded dispersion of a standard ridge waveguide mode. It sees the periodicity of the photonic crystal weakly, rather seeing an average refractive index. The influence of the photonic crystal is especially observed at the boundaries of the Brillouin zone where the dispersion slope is flattened and where a mini stop band opens up each time the mode is folded back into the first Brillouin zone. This mode is called the leaky refractivelike mode[5,6,8,11] because above 1.1×10^{14} Hz it leaks energy into the photonic crystal, when crossing regions where the density of crystal modes is high, and into air where it is located above the light line. Indeed, both can occur at the same time.

The second guided mode, labeled e_2, is a laterally odd mode and is located in the first bandgap of the photonic crystal.[9] By introducing the defect line into the photonic crystal, the e_2 mode is pulled down from the upper crystal band and therefore has the symmetry thereof. This mode is a truly photonic band-gap effect guided mode. Generally, below the light line this mode is expected to be guided with very low loss, often even through waveguide channels with sharp corners, since it lies within the photonic band gap. This mode is called the diffractivelike mode because its dispersion depends very strongly on the surrounding periodic structure of the crystal.[5,8,11]

The region encircled with a dotted rectangle in Fig. 4 indicates the measurement range shown in Fig. 3(a). We observe that the described refractivelike and diffractivelike guided modes are present in the measurement region. The refractivelike mode has a similar wave vector and field distribution to the fundamental mode of the ridge waveguide,[6] therefore the coupling from the ridge waveguide to this refractivelike mode is expected to be quite efficient, whereas the coupling efficiency from the ridge waveguide to the diffractivelike mode is expected to be very low because of the mode symmetry mismatch.[8]

The measured transmission spectrum of the straight photonic crystal waveguide [Fig. 3(a)] indicates efficient coupling from the ridge waveguide up to a frequency of 1.96×10^{14} Hz, which corresponds to about the lower edge of the mini stop band of the refractivelike mode in the dispersion diagram. Above the cutoff frequency the guided modes are either not available (e_1) or situated in regions where the density of photonic crystal states is high (e_2), therefore the mode from the ridge waveguide couples to the existing states of the photonic crystal, leaks energy into it and is no longer guided in the defect. This lack of light guidance corresponds to the very low measured transmission efficiency. These agreements between the measurements and the dispersion diagram confirm the coupling to the leaky refractive-like mode of the photonic crystal waveguide.

For low-loss transmission through a 90° bend waveguide a diffractivelike mode, which is located below the light line and in the photonic band gap, is desirable. A refractivelike mode is not expected to have a particularly high transmission efficiency around sharp bends. Since we have shown in the previous section that light from the ridge waveguide couples effectively into the refractivelike mode of the photonic crystal waveguide, a low transmission efficiency is expected. Nevertheless, the measured transmission spectrum of the 90° bend waveguide reaches nearly 90% at a frequency of 1.957×10^{14} Hz. Several observations in comparing the measurements and the dispersion diagram can give information as to why the observed high transmission efficiency is achieved. We observe that the frequency range of high transmission efficiency is situated close to the cutoff frequency of the straight photonic crystal waveguide, which corresponds to the mini stop band edge in the dispersion diagram. The cutoff frequency shift between the straight and the 90° bend waveguide is caused by fabrication-induced deviations in the crystal structure. In our simulations we have observed that the mini stop band edge position depends strongly on the design parameters. As mentioned already, the flattening of the dispersion slope approaching the mini-stop band edge

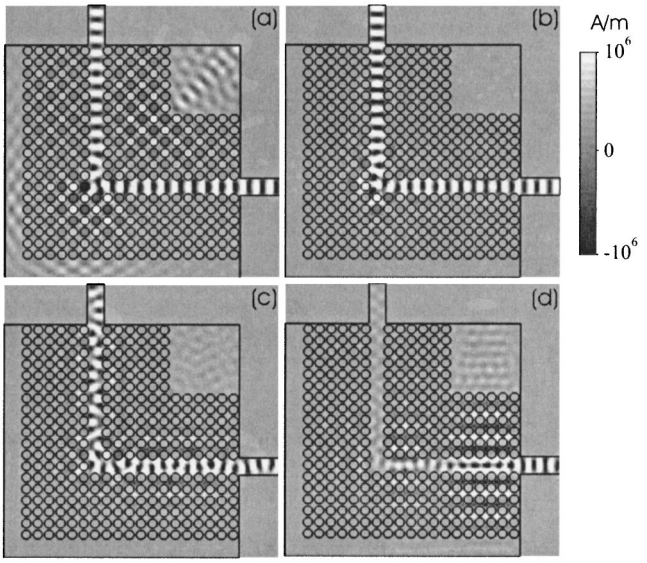

FIG. 5. Fully 3D simulated field distribution (magnetic field perpendicular to the photonic crystal membrane) of the light propagating around the 90° bend waveguide at different frequencies: (a) at $1.8614e^{14}$ Hz (b) at $1.9481e^{14}$ Hz (c) at $2.0286e^{14}$ Hz, and (d) at $2.0878e^{14}$ Hz.

indicates the increased effect of the photonic crystal structure on the refractivelike waveguide mode. Due to this increased effect of the photonic crystal structure, two positive observations in respect of the transmission efficiency can be made. First, drawing nearer to the mini stop band edge, Lončar *et al.* have observed that the propagation losses of the leaky refractivelike mode decrease.[7] Second, due to the flattened dispersion, the density of wave vectors of the propagating defect mode that are accessible for the light at the bend has increased, which makes an efficient change of propagation direction and high transmission around the 90° bend more probable. In addition, close to the edge of the Brillouin zone, the field distribution in the corner is such that an efficient coupling to the perpendicular photonic crystal waveguide is possible.

The fully 3D simulated field distribution (magnetic field perpendicular to the photonic crystal membrane) of the light propagating around the 90° bend waveguide is shown in Fig. 5 at different frequencies. At lower frequencies the e_1 mode behaves like an index-guided mode, which can be seen in Fig. 5(a). The light is well guided up to the bend, where it is then mostly reflected by the crystal, since the frequency of the light is situated in the range of the first photonic band gap. Only a small amount of light is guided around the bend. Increasing the frequency into the region where the dispersion slope flattens, the transmission efficiency around the bend increases due to the more diffractivelike character of the guided e_1 mode [Fig. 5(b)]. We also notice that at the bend a small amount of energy couples to the e_2 mode. However, it disappears after a few periods because according to the dispersion diagram e_2 couples to states of the photonic crystal and thus leaks energy into the crystal. Increasing the frequency close to the mini stop band edge, the ridge waveguide mode couples to the e_1 mode, which then couples in the corner to the several modes (beating in the field distribution) due to the broken symmetry matching the field distribution at the corner Fig. 5(c). Among others, the e_2 mode can be identified in both of the waveguide branches. One part of the e_2 mode is guided around the bend to the exiting ridge waveguide whereas the other part is reflected in the corner. Due to the low modal conversion efficiency between the e_1 and the e_2 modes the transmission efficiency decreases. The discussed modal conversion could be an interesting point of study. Since the e_2 mode is truly photonic band-gap effect guided and therefore is preferable to the e_1 mode for low loss guiding, it might be possible to design a waveguide that deliberately breaks the symmetry of the e_1 mode in order to couple to e_2 mode. Efficient modal conversion from a ridge waveguide mode to the e_1 mode and then to the e_2 mode might then be achieved. At the frequency of $2.08*10^{14}$ Hz no propagating mode exists outside of regions with a high density of photonic crystal states, therefore light couples to the photonic crystal modes and is no longer confined within the defect [Fig. 5(d)]. The comparison of the measurements with the dispersion diagram and the field simulation has shown that the measured maximum transmission efficiency is mainly associated with the leaky refractivelike mode, whereas the small peaks above the cutoff frequency, seen in both experiment and theory, are associated with weak coupling to the diffractive-like mode.

III. CONCLUSIONS

To conclude, by comparing different designs of waveguides with 3D calculation, we have identified the guided modes propagating around the 90° bend waveguide. High transmission efficiency was achieved with the leaky refractivelike mode. Despite the vertical losses, the leaky refractivelike mode presents some interesting advantages for short photonic crystal waveguide sections. Due to the good modal matching, a high coupling efficiency is observed between the conventional ridge waveguide and the photonic crystal waveguide mode. We have shown that the refractivelike mode can also be guided effectively around sharp bends close to the mini stop band at the boundary of the Brillouin zone where the dispersion slope in the band diagram becomes flatter and the mode gains a more diffractivelike character. Further improvement of the transmission efficiency should be possible by reducing the sidewall roughness of the photonic crystal. By optimizing the design of the 90° bend, by restructuring the layout of the corner, it should be possible to broaden the transmission bandwidth.[21,22] The presented results prove that the leaky refractivelike mode can be used in devices containing short photonic crystal sections and can exhibit quite high transmission efficiencies even around sharp waveguide bends.

ACKNOWLEDGMENTS

The authors acknowledge F. Schädelin, S. Gautsch, U. Staufer, and P.-A. Künzi for useful discussions and for fabricating the photonic crystal waveguide samples. Furthermore, the authors thank R. Stanley of the Swiss Center of Electronics and Microtechnology (CSEM) for fruitful discus-

sions. This work is funded under a joint projects program between the Swiss Center of Electronics and Microtechnology (CSEM) and the IMT-Uni Neuchâtel.

[1] S. G. Johnson, P. R. Villeneuve, S. Fan, and J. D. Joannopoulos, Phys. Rev. B **62**, 8212 (2000).
[2] M. Lončar, J. Vučković, and A. Scherer, J. Opt. Soc. Am. B **18**, 1362 (2001).
[3] M. D. B. Charlton, M. E. Zoorob, G. J. Parker, M. C. Netti, J. J. Baumberg, S. J. Cox, and H. Kemhadjian, Mater. Sci. Eng., B **74**, 17 (2000).
[4] S. Y. Lin, E. Chow, S. G. Johnson, and J. D. Joannopoulos, Opt. Lett. **25**, 1297 (2000).
[5] M. Lončar, T. Doll, J. Vučković, and A. Scherer, J. Lightwave Technol. **18**, 1402 (2000).
[6] A. Adibi, Y. Xu, R. K. Lee, A. Yariv, and A. Scherer, J. Lightwave Technol. **18**, 1554 (2000).
[7] M. Lončar, D. Nedeljković, T. P. Pearsall, J. V. Vučković, A. Scherer, S. Kuchinsky, and D. C. Allan, Appl. Phys. Lett. **80**, 1689 (2002).
[8] Y. Désières, T. Benyattou, R. Orobtchouk, A. Morand, P. Benech, C. Grillet, C. Seassal, X. Letartre, P. Rojo-Romeo, and P. Viktorovitch, J. Appl. Phys. **92**, 2227 (2002).
[9] X. Letartre, C. Seassal, C. Grillet, P. Rojo-Romeo, P. Viktorovitch, M. Le Vassor d'Yerville, D. Cassagne, and C. Jouanin, Appl. Phys. Lett. **79**, 2312 (2001).
[10] S. Kuchinsky, D. C. Allan, N. F. Borelli, and J.-C. Cotteverte, Opt. Commun. **175**, 147 (2000).
[11] A. Mekis, J. C. Chen, I. Kurland, S. Fan, P. R. Villeneuve, and J. D. Joannopoulos, Phys. Rev. Lett. **77**, 3787 (1996).
[12] E. Chow, S. Y. Lin, J. R. Wendt, S. G. Johnson, and J. D. Joannopoulos, Opt. Lett. **26**, 286 (2001).
[13] A. Talneau, L. Le Gouezigou, N. Bouadma, M. Kafesaki, C. M. Soukoulis, and M. Agio, Appl. Phys. Lett. **80**, 547 (2002).
[14] M. Tokushima, H. Kosaka, A. Tomita, and H. Yamada, Appl. Phys. Lett. **76**, 952 (2000).
[15] A. Chutinan, M. Okano, and S. Noda, Appl. Phys. Lett. **80**, 1698 (2002).
[16] Y. Sugimoto, N. Ikeda, N. Carlsson, K. Asakawa, N. Kawai, and K. Inoue, J. Appl. Phys. **91**, 3477 (2002).
[17] C. C. Cheng and A. Scherer, J. Vac. Sci. Technol. B **13**, 2696 (1995).
[18] E. Miyai, M. Okano, M. Mochizuki, and S. Noda, Appl. Phys. Lett. **81**, 3729 (2002).
[19] T. Weiland, Int. J. Numer. Modelling: Electronic Networks, Devices and Fields **9**, 295 (1996).
[20] S. G. Johnson and J. D. Joannopoulos, Opt. Express **8**, 173 (2001).
[21] A. Chutinan, M. Okano, and S. Noda, Appl. Phys. Lett. **80**, 1698 (2002).
[22] J. Smajic, C. Hafner, and D. Erni, Opt. Express **11**, 1378 (2003).